

Organic Host Encapsulation Effects on Nitrosobenzene Monomer–Dimer Distribution and C–NO Bond Rotation in an Aqueous Solution

Ramkumar Varadharajan, Sarah Ariel Kelley, Vindi M. Jayasinghe-Arachchige, Rajeev Prabhakar, Vaidhyathan Ramamurthy,* and Silas C. Blackstock*



Cite This: *ACS Org. Inorg. Au* 2022, 2, 175–185



Read Online

ACCESS |



Metrics & More

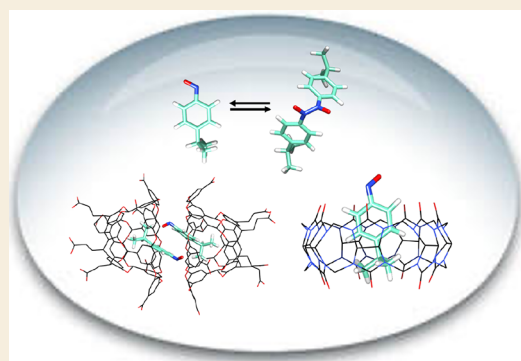


Article Recommendations



Supporting Information

ABSTRACT: The intermolecular (monomer–dimer equilibrium) and intramolecular (C–NO and C–NMe₂ rotations) dynamics of 4-nitrosocumene (**1a**) and 4-(*N,N*-dimethylamino)nitrosobenzene (**1b**), respectively, were found to be controlled by the medium (water) and the host environment (organic capsules and cavitands). The ability of water to shift the equilibrium toward the dimer appears to result from dipolar stabilization of the polar dimer structure and has a resemblance to water's known ability to favor organic cycloaddition reactions. In an aqueous medium, a range of organic hosts selectively include only the nitrosocumene monomer **1a**. Encapsulation in the octa acid duplex (OA₂) selects two **1a** monomers rather than a dimer structure. Octa acid encapsulation also results in more restricted intramolecular C–N rotations of the guest **1b**.



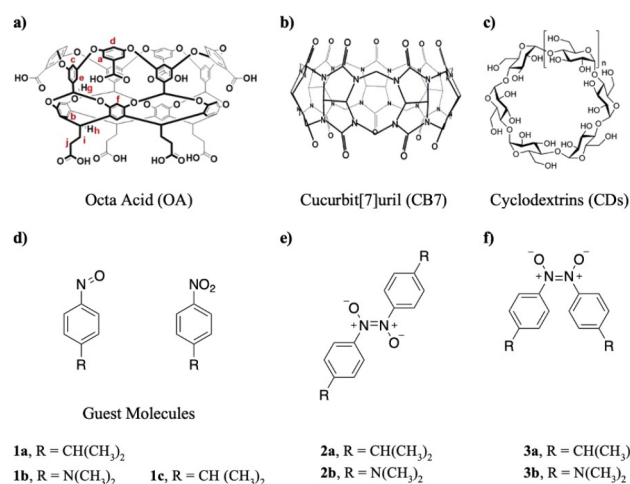
KEYWORDS: nitrosobenzenes, octa acid, cucurbit[7]uril, cyclodextrins, host–guest complexation, monomer–dimer equilibrium, C–N bond rotation

INTRODUCTION

Supramolecular chemistry continues to play an important role in unraveling the hidden structural features of organic molecules.^{1–4} In this article, we present the results of our experiments probing the dynamic covalent bonding characteristics of the C-nitroso function, a less investigated chromophore, incarcerated in the small well-defined space provided by the organic carcerands octa acid (OA), cyclodextrin (CD), and cucurbituril (CB) (Scheme 1).^{4–6} The above three water-soluble cavitands have internal cavities with similar features and dimensions and internal polarities conducive for hosting hydrophobic organic guests in water. However, they differ in the functionality (COOH, OH, and C=O) present on the rims, which might interact differently with the guest nitroso compounds. In addition, while CD and CB form open host complexes (carceplexes), OA forms both open and closed complexes (carceplexes and capsuleplexes) with guest molecules. We were interested in exploring the influence of the restricted space provided by the above three hosts on the intermolecular (monomer–dimer equilibrium) and intramolecular (C–NO and C–NMe₂ σ -bond rotations) dynamics of two nitroso benzene derivatives **1a** and **1b** (Schemes 1 and 2).^{7–12}

The dynamic covalent bonding of nitrosobenzenes is a novel self-assembly property of this organic function.^{7,8} Nitrosobenzenes, in the neat form, typically exist as covalently

Scheme 1. Chemical Structures of (a–c) Host and (d–f) Guest Molecules



Received: November 1, 2021

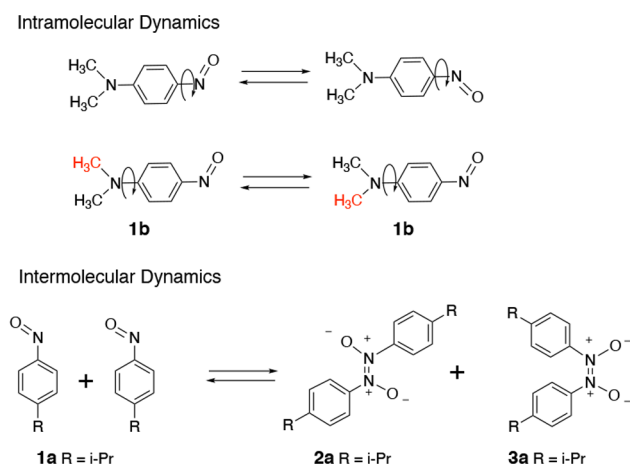
Revised: November 30, 2021

Accepted: November 30, 2021

Published: December 22, 2021



Scheme 2. Intra- and Intermolecular Dynamics Probed in this Study



bonded azodioxide dimers, which dissociate readily and reversibly to monomeric structures in solution (Schemes 1 and 2). The monomeric form is easily identified by its blue or green color.¹³ In the monomer, rotation about the C–NO bond is fast on the NMR time scale.¹⁴ Substitution at the 4-position by electron-donating groups slows the C–NO bond rotation and diminishes the propensity for nitrosobenzene dimerization.^{14,15} This prompted us to select 4-nitrosocumene (**1a**) and 4-(*N,N*-dimethylamino)nitrosobenzene (**1b**) as probe molecules to investigate the influence of supramolecular effects on the inter- and intramolecular dynamics of molecules possessing nitroso chromophores.

RESULTS AND DISCUSSION

Figure 1 shows the ¹H NMR spectra of **1a** in several organic solvents (i–iii) and D₂O (iv–vii) at a range of concentrations (Figure S1). In CDCl₃, methanol-*d*₄, and DMSO-*d*₆, **1a** exists exclusively in its monomeric form (M) at a 2 mM

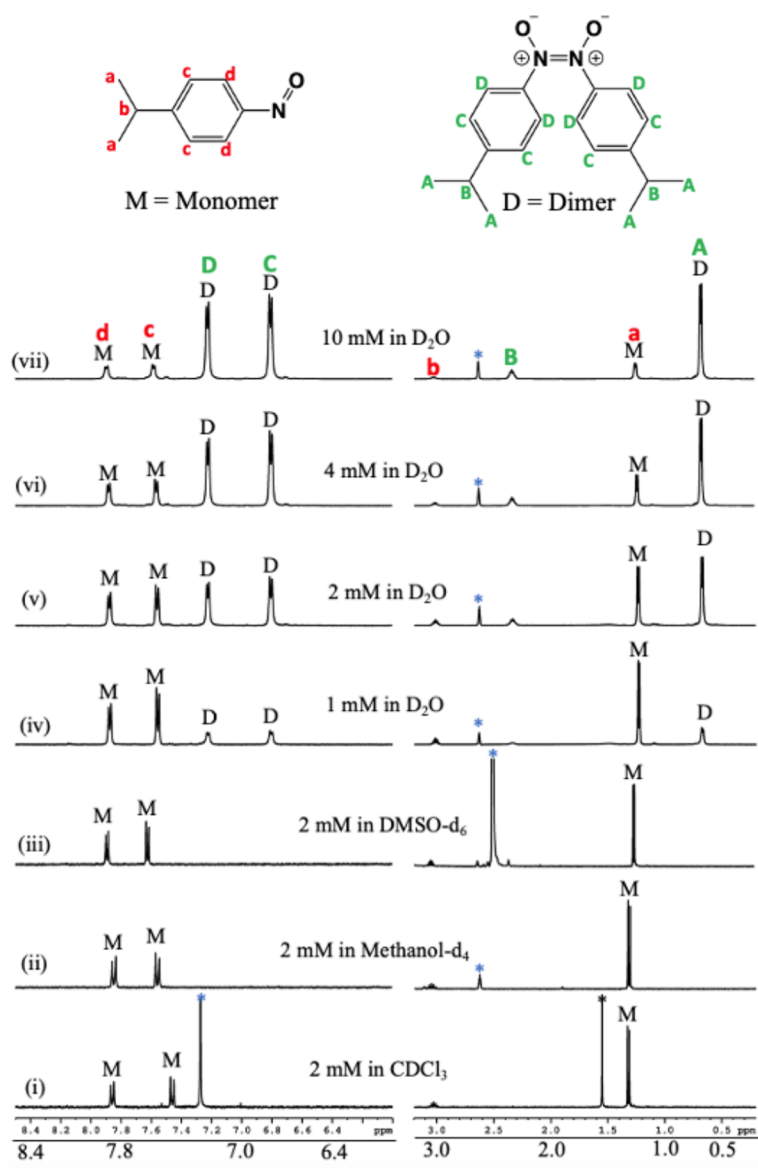
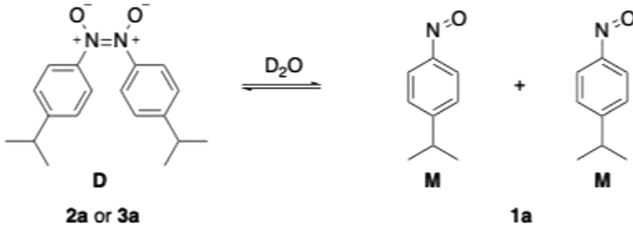


Figure 1. ¹H NMR partial spectra (500 MHz) of **1a** in (i) CDCl₃ (ii) methanol-*d*₄ (iii) DMSO-*d*₆ and (iv)–(vii) D₂O. M and D indicate the monomer and dimer signals, respectively, and the asterisk (*) and star (*) mark residual protio solvents and HOD peaks, respectively.

concentration at room temperature for this set of solvents of widely ranging polarity. Even if the concentration of **1a** is increased to 10 mM, only the monomer is observed in these solvents (Figures S5–S7). In contrast signals due to the dimer (D) are present in D₂O even at a 1 mM concentration (Figures 1 and S1). As the concentration increases, the amount of dimer signal in the equilibrium increases, reaching 84% at 10 mM. Solutions become turbid at the higher concentrations, but the ¹H NMR signals remain sharp. As seen in Table 1, the total

Table 1. 1a Concentration Study in D₂O (NaOAc Internal Standard)



[total 1a] in D ₂ O (mM) added to NMR tube	concentrations (mM)				
	[M]	[D]	[sodium acetate]	[total 1a observed] ^a ([M]+2[D])	K _m (M)
2.9	0.63	0.68	9.8	2.0	5.9 × 10 ⁻⁰⁴
3.9	0.63	0.9	9.7	2.4	4.4 × 10 ⁻⁰⁴
4.8	0.68	1.3	9.6	3.4	3.4 × 10 ⁻⁰⁴
6.6	0.71	2.2	9.4	5.1	2.3 × 10 ⁻⁰⁴
9.2	0.83	3.2	9.2	7.2	2.2 × 10 ⁻⁰⁴
average				3.6 × 10 ⁻⁰⁴ ± 1.5 × 10 ⁻⁰⁴	

^aThe value of [total **1a** observed] does not equal [total **1a**] values, which is likely due to increasing turbidity of solution at higher concentrations that may reflect the formation of higher-order aggregates.

concentration of M and D is less than the total amount of **1a** dissolved, especially at high concentrations. This is likely due to aggregation, but we currently do not have experimental support for this aspect. Employing an internal standard, we found $K = 3.6 \pm 1.6 \times 10^{-4}$ M and $\Delta G^\circ = 20 \pm 1$ kJ/mol at 27 °C for the **1a** D–M equilibrium in D₂O using quantitative ¹H NMR analysis (see Table 1 and Figures S3 and S4). For comparison, we note that for the parent nitrosobenzene, Ph–NO, in CD₂Cl₂ at 25 °C has values of $K = 52$ and $\Delta G^\circ = -9.8$ kJ/mol.^{15,16} Thus, we observe a large medium effect on the order of 10⁵ in K for monomerization between organic solvent (monomer favored) and water (dimer favored). We believe that the hydrophobic effect is likely a factor that favors the dimer in water along with the preferential aqueous stabilization of the dipolar dimer structure.^{17–30}

Having established the preference of **1a** in water to be a dimer with the monomer also present, we were curious to examine whether it would be possible to alter the equilibrium in water without involving the mixed solvent strategy. This led us to probe the effect on the D–M equilibrium of including **1a** in the restricted hydrophobic cavity provided by water-soluble hosts OA, CD, and CB7 (Scheme 1). Given the large polarity difference between nitrosocumene's M (**1a**) and D (**2a** and **3a**) forms, we anticipated that a nonpolar organic host enclosure might preferentially recruit the less polar M nitrosocumene rather than its dipolar D structural form. On

the other hand, in the case of the large enclosure space of the OA₂ capsule, it is possible that multiple guests could be encapsulated, which could favor D formation at a very high local M guest concentration. Thus, three factors, namely the internal polarity, the local concentration, and the restricted space, are likely to play a role in controlling the D–M equilibrium. The results of this study should have relevance to biological systems, where (similar to the current situation) while the chemistry as a whole occurs in water, the specific activity may occur in a well-defined hydrophobic restricted space.

We first investigated the effect of OA on the D–M equilibrium of **1a**. Upon mixing the OA host and nitrosocumene guest in an aqueous solution, the NMR signals of both components were redistributed, suggestive of H:G binding. When nitrosocumene was incrementally titrated into an excess of aqueous OA, as shown in Figure 2 (and Figures S8 and S9), the NMR data suggest that two types of complexes form depending on the OA:guest (H:G) ratio.³¹ At low concentrations of the guest compared to the host, a broad singlet at δ ca. -0.9 ppm appears and is assigned as the *i*-Pr methyl Hs of a **1a**@OA₂ complex. As the **1a** concentration increases beyond a H:G ratio of 2:0.8 (Figure 2, spectra 10–13), the NMR signal at -0.9 ppm diminishes while a new broad singlet at δ ca. -1.9 ppm emerges and reaches a maximum value at a H:G (OA:**1a**) ratio of 2:2. We assign the broad singlet at -1.9 ppm to the *i*-Pr methyl groups of a **1a**₂@OA₂ complex in which two **1a** units are enclosed in a single OA₂ capsule. It is worth noting that the restricted rotation of the *i*-Pr methyl groups within the OA capsule renders the doublet signal into a broad singlet. As expected, the direct formation of only the H:G 2:2 **1a**₂@OA₂ complex occurs when OA is added incrementally to a solution of excess **1a** (Figures 3, S13, and S14). The formation of the OA₂ capsuleplex was confirmed by the measured diffusion constant of 1.39×10^{-6} cm²/s determined from DOSY experiments (Figure S11).^{31,32}

The above NMR results do not indicate whether the bound guest signals at δ -0.9 and -1.9 ppm are due to *i*-Pr methyl groups of the monomer **1a** or the dimer azodioxide **2a** and **3a** structures (Scheme 1). Confirmatory evidence in favor of the monomer comes from the visible absorption spectra displayed in Figure 4. The 2:2 H:G complex possesses a broad absorption between 600 and 850 nm due to the $n \rightarrow \pi^*$ transition characteristic of a nitrosoarene monomer.¹³

According to molecular dynamics (MD) simulated structures shown in Figure 5, the following three complexes are possible: **1a**@OA₂, (**1a**)₂@OA₂, and **2a**@OA₂. MD simulations of the (*Z*)-dimer **3a** within OA resulted in conversion to dimer **2a** within a few nanoseconds, suggesting that **3a** is not viable within the OA capsule. Despite there being sufficient space within the OA cavity to accommodate dimer **2a**, the OA-bound guests exist only as monomers of **1a** even at the very high local monomer concentration of ~5 M (estimated from two **1a** molecules in the 650 Å³ cavity interior) in the OA₂ capsule.³³ The fact that only monomers are present within the OA capsule suggests that the dimer present in solution enters the capsule in the form of a monomer. Apparently, the monomer present in the equilibrium is selectively included within the OA capsule, and the equilibrium shifts eventually to only the monomer. Why do the two monomers present in a small space not dimerize? Dimerization of nitroso compounds is thought to occur via a non-least-motion process in which the C–N=O functions first approach each other in perpendicular

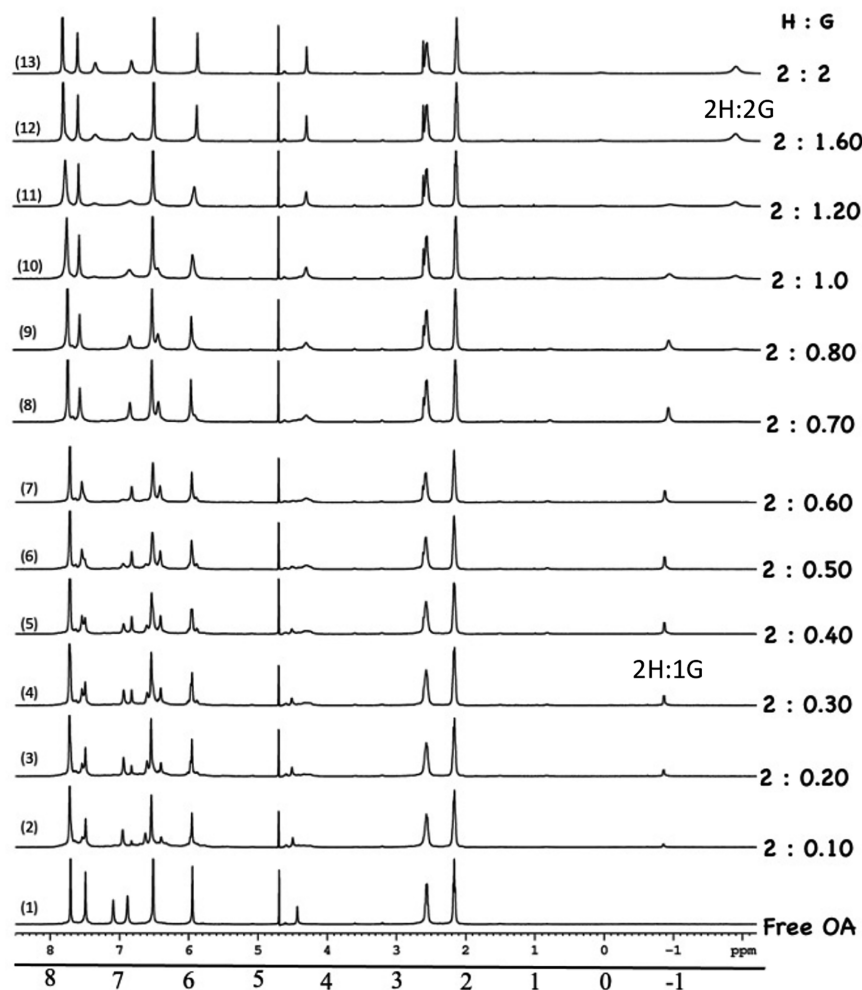


Figure 2. ^1H NMR spectra (500 MHz, D_2O) of (1) host-only $[\text{OA}] = 5$ mM and (2–13) $[\text{OA}] = 5$ mM and guest $[\mathbf{1a}] = 0.25, 0.5, 0.75, 1.0, 0.125, 1.5, 1.75, 2.0, 2.5, 3.0, 4.0,$ and 5.0 mM, respectively. The signals at $\delta -0.9$ and -1.9 ppm are attributed to the *i*-Pr group of the 2:1 and 2:2 H:G complexes, respectively.

planes³⁴ and ultimately yield a transition structure for E-dimer formation having R–NO groups offset in parallel planes to foster FMO interactions, as modeled by HNO dimerization calculations (Scheme 3).^{35–37} Given the space limitations of the OA_2 cavity, we cannot rule out the kinetic inhibition of dimerization in the OA capsule. However, it seems likely that the large differences in polarity and H-bonding properties between the polar water medium and the nonpolar aromatic ring-lined interior of OA ³⁸ are responsible for the dramatic change of the $\mathbf{1a}$ aggregation state in the two “inside capsule” and “outside capsule” environments.

It is interesting to note the counterintuitive direction of the monomer versus dimer preference in this case, where the dimer is favored in the dilute (aqueous) solution and the monomer is favored in the highly concentrated confines of the nonpolar OA_2 capsule. Given that $\mathbf{1a}$ prefers to be a dimer in water, its existence as a monomer under such high concentrations in a small space floating in an aqueous medium was unanticipated, probably reflecting the roles of micro-polarity and restricted space in controlling the D–M equilibrium in favor of M within the OA capsule.

Finally, we note that the M–D equilibrated structures of Figure 5 helps rationalize the chemical shift difference of the isopropyl methyl signals for $\mathbf{1a}@\text{(OA)}_2$ and $(\mathbf{1a})_2@\text{(OA)}_2$

complexes, with the $\mathbf{1a}$ guest of the latter complex having a deeper cavity penetration by the isopropyl group and hence greater shielding by the interior aromatic rings near the base of the OA cavity.

Having established the monomer $\mathbf{1a}$'s preference for encapsulation by the OA capsule, we were interested in examining the binding preferences of open cavitandplexes CD and CB. For these hosts, since the cavitands do not form capsules like OA, the partially confined guest molecules are exposed to water from the top and bottom of the cavitand. This feature allows us to examine whether the presence of water molecules surrounding the mouths of the CD and CB cavitandplexes would favor the dimer instead of the monomer within the cavities of CD and CB. As observed with OA, the addition of α -, β -, or γ -CD hosts results in the formation of host–guest complexes that perturb the nitrosocumene monomer–dimer equilibrium. Increasing the amounts of α -, β -, and γ -CD cavitands leads to a decrease and broadening of the nitrosobenzene dimer NMR signals (Figures S15–S26). Figure 6 displays the monomer (M) and dimer (D) aromatic H NMR signals observed upon the incremental addition of γ -cyclodextrin to aqueous nitrosocumene. The loss of the dimer signal as the amount of the host added increases is consistent with selective binding of the $\mathbf{1a}$ monomer and a shifting of the

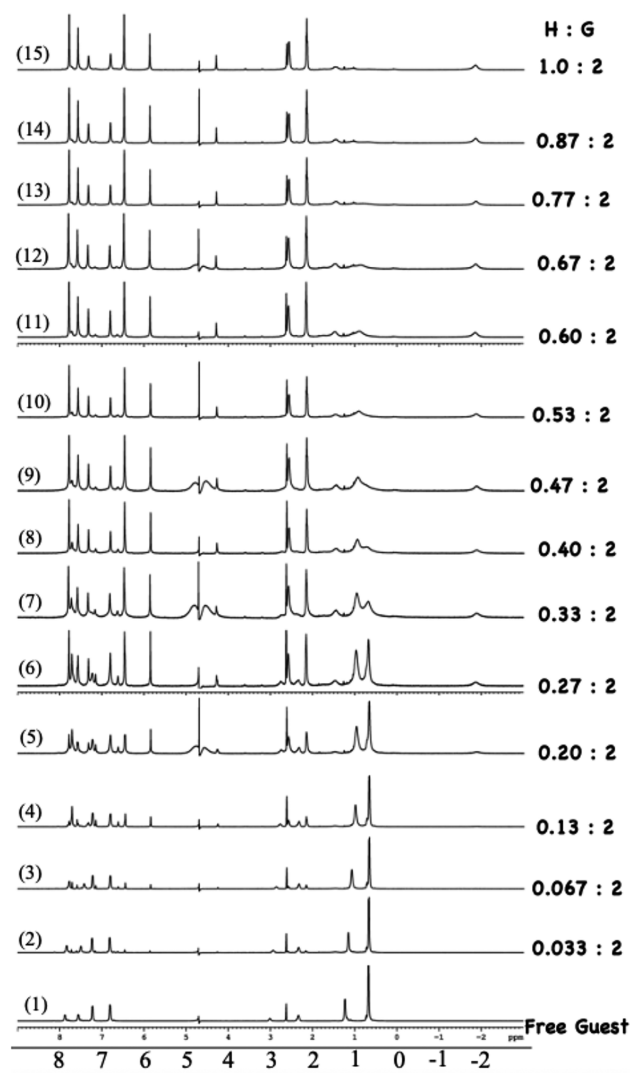


Figure 3. ^1H NMR spectra (500 MHz, D_2O) of (1) guest-only [$\mathbf{1a}$] = 3 mM and (2–15) guest [$\mathbf{1a}$] = 3 mM with added host [OA] = 0.05, 0.1, 0.2, 0.3, 0.4, 0.5, 0.6, 0.7, 0.8, 0.9, 1.0, 1.2, 1.3, and 1.5 mM, respectively. The signal at δ -1.9 ppm is attributed to the *i*-Pr group of the 2:2 H:G complex.

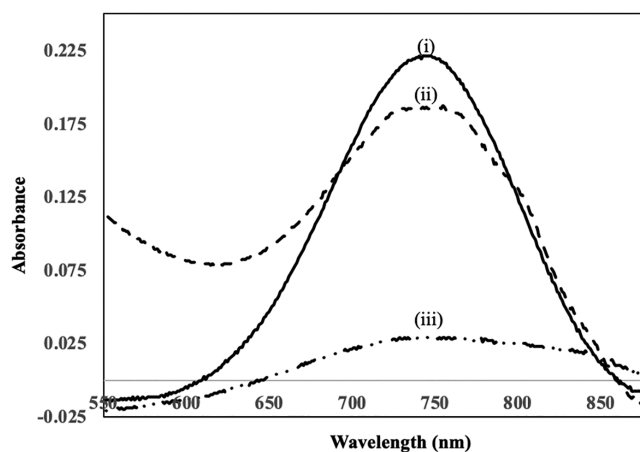


Figure 4. Absorption spectra of $\mathbf{1a}$ (5×10^{-3} M, $n \rightarrow \pi^*$ region) in (i) chloroform, (ii) aqueous OA (5×10^{-3} M), and (iii) water.

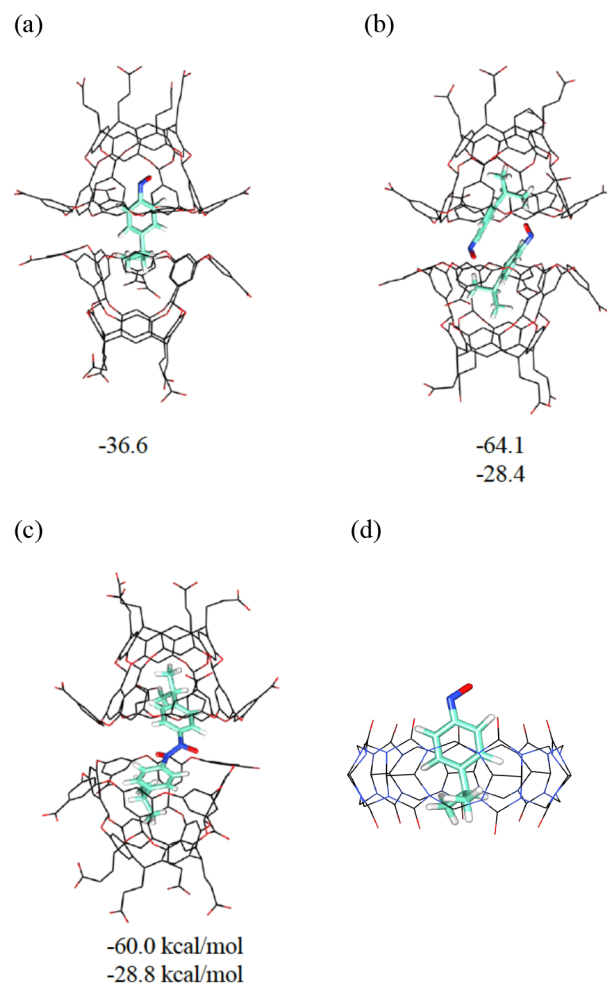
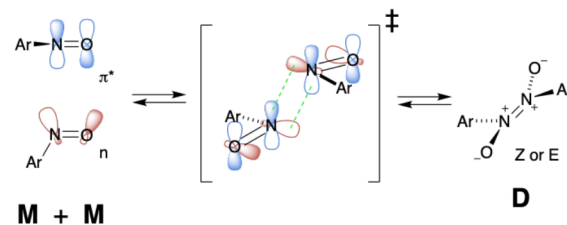


Figure 5. Structures of (a) $\mathbf{1a}@(\text{OA})_2$, (b) $(\mathbf{1a})_2@(\text{OA})_2$, and (c) $\mathbf{2a}@(\text{OA})_2$ computationally generated by molecular dynamics calculations, with binding free energies (kcal/mol) computed by the MMPBSA method (first line) and the λ -particle approach (second line). (d) A computationally generated structure of 1:1 H:G of CB7:1a.

Scheme 3. Likely Pathway for the Dimerization of Nitrosobenzene with FMO Interactions



monomer–dimer equilibrium to ultimately deplete dimeric structures. Small shifts in the host CD NMR signals, compared to signal positions observed in pure aqueous CD solutions were also observed (Figures S17, S21, and S25), indicative of proposed $\mathbf{1a}$ –CD complex formation. In these cases, preferential CD binding of monomer $\mathbf{1a}$ over dimers $\mathbf{2a}$ and $\mathbf{3a}$ presumably reflects the cavity's dimensional preference for the monomer structure as well as the selection based on the less polar monomeric $\mathbf{1a}$ compared to the dipolar dimer

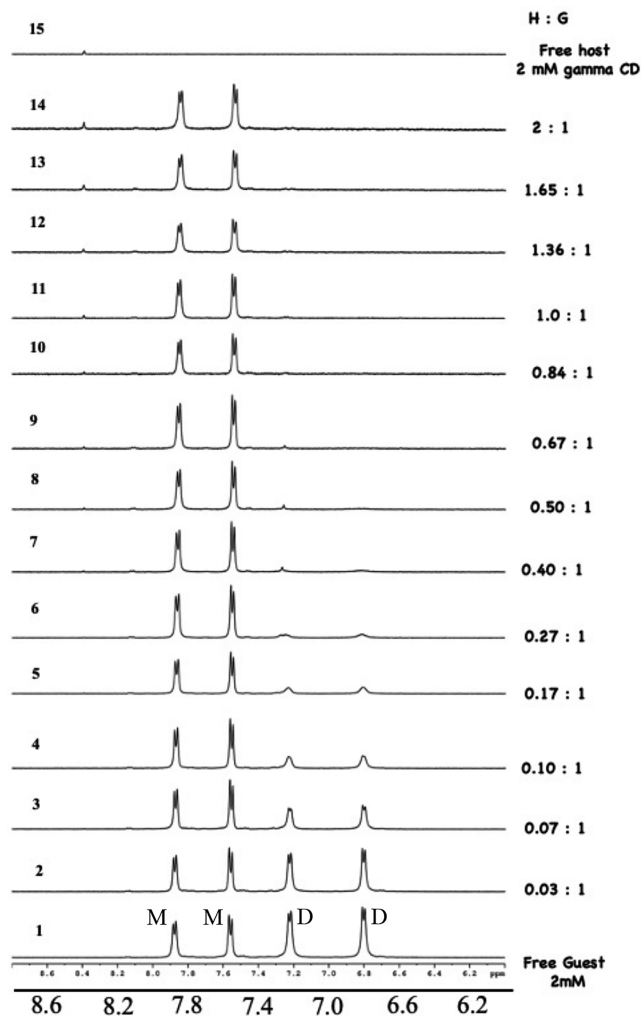


Figure 6. ^1H NMR spectra of aromatic region for (1) 2.0 mM aqueous *p*-nitrosocumene, (2–14) 2.0 mM aqueous *p*-nitrosocumene with an added γ -cyclodextrin host, and (15) 2.0 mM free host.

structure(s), as also observed for the OA binding of nitrosocumene **1a**.

Similar to OA and CD, cavitand CB7 was also found to be an effective host for the nitrosobenzene monomer **1a**. The ^1H NMR spectra of CB7 complexes display some interesting and unusual features (Figures 7 and S27–S30). When nitrosocumene was added to an excess amount of the aqueous host CB7 (H:G 4:1), a single set of NMR signals for the nitrosobenzene were observed and assigned to CB7-bound **1a** monomer (Figure 7i). Upon the addition of more of the nitrosocumene guest to give H:G ratios of 2:1 and ultimately 1:1, the isopropyl methyl signal (δ 0.55 ppm) and one of the aromatic hydrogen signals (δ 6.42 ppm) broadened substantially (Figures 7ii and iii and S27–S30), suggesting the occurrence of the dynamic exchange of the guest in and out of the CB7 host. The computationally generated structure shown in Figure 5d helps explain the broadening of only two of the guest NMR signals. The **1a**@CB7 complex model suggests that the isopropyl and adjacent aromatic hydrogens of **1a** are included within the interior of the CB7 host, and these hydrogens would experience the largest effect of guest exchange in and out of the CB7 cavity and hence their signals would broaden the most. To rule out the involvement of the

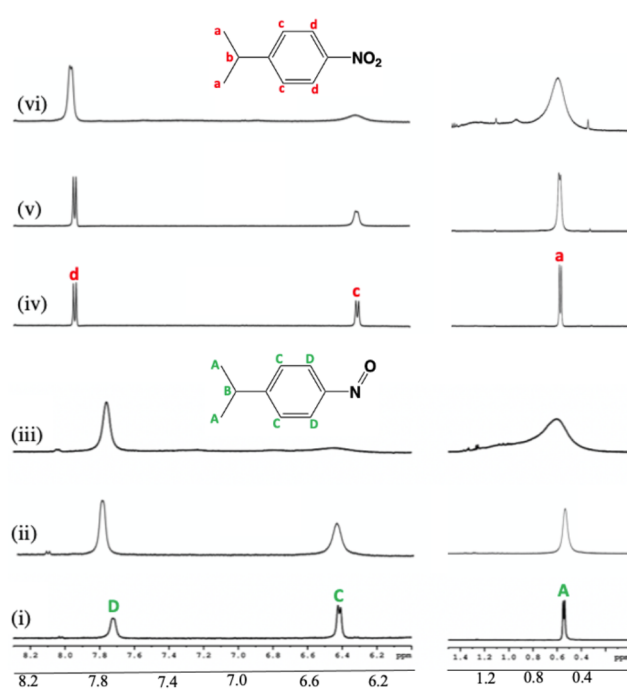


Figure 7. ^1H NMR spectra (500 MHz, D_2O) of the CB7 host (2×10^{-3} M) with the following guests: (i) (H:G 4:1) [**1a**] = 0.50×10^{-3} M, (ii) (H:G 2:1) [**1a**] = 1.0×10^{-3} M, (iii) (H:G 1:1) [**1a**] = 2.0×10^{-3} M, (iv) (H:G 4:1) [**1c**] = 0.50×10^{-3} M, (v) (H:G 2:1) [**1c**] = 1.0×10^{-3} M, and (vi) (H:G 1:1) [**1c**] = 2.0×10^{-3} M.

dimer (**2a** or **3a**) in the exchange and broadening process, we evaluated the analogous *p*-nitrosocumene structure **1c** as a **1a** monomer model that cannot exist in dimer form. Indeed, **1c**, whose polarity and footprint are similar to those of the **1a** monomer, gives analogous NMR signal shifts and broadening when exposed to CB7 (Figure 7iv–vi), providing support for the assignment of the **1a**@CB7 complex formation and exchange process. Finally, we note that for all CD and CB7 complexes of **1a**, the $n \rightarrow \pi^*$ absorption in the visible spectrum was observed, thus supporting the assignment of the monomeric complex formation of **1a**@CD and **1a**@CB7 (Figure S31).

In a separate study, we next evaluated host effects on the C–NO bond rotation dynamics of 4-(*N,N*-dimethylamino)-nitrosobenzene **1b**, which was chosen because its rates are measurable by NMR analysis at 2–52 °C in water. This molecule gave us an opportunity to examine the role of space on the intramolecular dynamics of freely rotating σ -bonds. Unlike **1a**, nitrosobenzene **1b** exists only as a monomer in water. Similar to **1a**, **1b** forms 2:1 and 2:2 H:G complexes with the OA host, the latter being more stable (Figures S32–S35). The methyl NMR signal of **1b** shifts from δ 3.3 ppm in water to 1.1 ppm in the 2:1 H:G complex and 0.3 ppm in the 2:2 H:G complex (Figures S32 and 33, respectively). Consistent with OA capsule formation, the diffusion constant of the 2:2 complex was found to be 1.43×10^{-6} cm^2/s by DOSY experiments (Figure S36).^{31,32} Computationally modeled structures for 2:1 and 2:2 OA:**1b** complexes are similar to those for **1a** (Figure S39), suggesting that both types of complexes are feasible. Interestingly, it is noted that both $n \rightarrow \pi^*$ and $\pi \rightarrow \pi^*$ optical transitions are solvent dependent for **1b** (Figures 8 and S40–S42 and Table S1). Upon inclusion within OA, both **1b** transitions shift from the water position to that

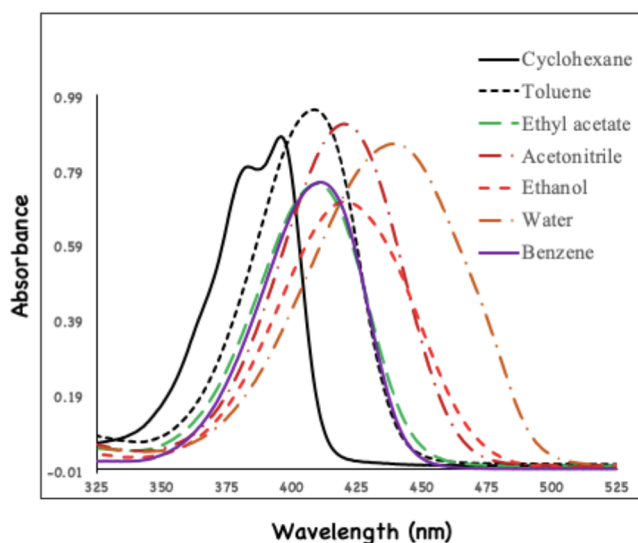
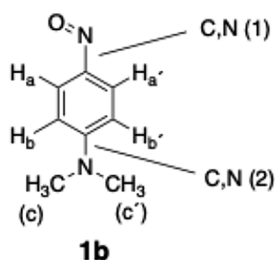


Figure 8. UV–visible absorption spectra ($\pi \rightarrow \pi^*$ region) of **1b** in different solvents. See Figure S42 for absorption within OA.

observed for a benzene solvent (Figure S42), suggesting a benzene-like internal polarity of the OA capsule that is in agreement with the earlier studies using fluorescent and EPR probes.³⁸

The extensive delocalization of the lone pair of the *N,N*-dimethyl amino group into the aromatic ring and the nitroso group has the effect of slowing the bond rotations of both C–NMe₂ and C–NO. This is evident from the variable temperature (VT) experiments carried out with **1b** both in water and included in the OA capsule. Results are summarized in Table 2 and Figures 9 and S43–S45. In water at 2 °C

Table 2. **1b** VT-NMR C–N Bond Rotational Data in D₂O and OA



NMR signals	$\Delta\nu$ (Hz)	T_c (K)	ΔG^\ddagger C, N (1) (kJ/mol)	ΔG^\ddagger C, N (2) (kJ/mol)
in D ₂ O				
H _{a,a'}	535	325		
H _{b,b'}	50	298	61.1 (298 K)	
H _{c,c'}				fast ^a
in OA				
H _{a,a'}	575	318		
H _{b,b'}	50	293	60.2 (293 K)	
H _{c,c'}	55			59.8 (293 K)
in CDCl ₃ ³⁹				
			54.4 (293 K) ³⁶	
in tol- <i>d</i> ₈ ^{39,b}				
			52.4 (293 K), ^{36b}	

^aShared singlet observed by VT-NMR. ^bFor 4-(diethylamino)-nitrosobenzene.

(Figure 9a), independent signals for all four aromatic hydrogens were observed, while the –NMe₂ signal remained a sharp singlet. This is consistent with fast (averaged) C–NMe₂ bond rotation and slow (frozen) C–NO bond rotation on the NMR time scale under these conditions. The derived C–NO bond rotation barrier in D₂O gives ΔG^\ddagger (298 K) = 61.1 kJ/mol (Table 2). In OA, the NMR spectra of **1b** are distinctly different (Figures 9b and S45). At 2 °C, NMR signals for the four aromatic hydrogens and the two *N*-methyl groups are distinctly visible, indicating slow (frozen) bond rotations for both C–NMe₂ and C–NO on the NMR time scale at this temperature in the OA cavity. The *N*-methyl signals and the two upfield aromatic hydrogen signals both coalesce at ~293 K, yielding approximate ΔG^\ddagger (293 K) C–N rotation barriers of 60.2 and 59.8 kJ/mol, respectively, for C–NO and C–NMe₂ within OA (Table 2).

Two features of the above results are noteworthy. First, there is a large solvent medium effect on **1b**'s C–NO bond rotation barrier, with ΔG^\ddagger (298 K) in D₂O being ~8 kJ/mol higher than that in the aprotic nonpolar CDCl₃ solvent for which ΔG^\ddagger (298 K) values of 52.8 and 53.6 kJ/mol have been reported.³⁹ We hypothesize that ground-state stabilization by hydrogen bonding of water to the planar dipolar quinonoid structure of **1b**, along with water dipolar stabilization of the structure, raises the rotational barrier in water. Second, despite the nonpolar interior of the OA capsule, the C–NO rotation rate of **1b** in the OA capsule remains nearly as slow as that in the D₂O medium and much slower than in the nonpolar chloroform or toluene solvent, which are better models of the OA cavity polarity (Table 2). We suspect that the confined space of the OA capsule raises the C–NO rotation barrier above that expected for its nonpolar interior. Consistent with this notion is the notable restricted rotation of the C–NMe₂ group, which always remains freely rotating (i.e., time-averaged on the NMR time scale) in bulk solution. Given the essentially equal barriers to C–NO and C–NMe₂ rotation observed in the OA capsule, it seems likely that the –NMe₂ group is “anchored” in the OA host and does not freely rotate on the NMR time scale in this environment such that the methyl groups are rendered inequivalent by the slowed C–NO rotation at low temperatures. Such a clean spectrum (Figure 9b(i)) with independent signals for all hydrogens of OA-bound **1b** is noteworthy.

CONCLUSIONS

In this study, we have demonstrated that supramolecular features of organic hosts can be utilized to manipulate the inter- and intramolecular dynamics of guest molecules. The *p*-alkyl-substituted nitrosobenzene **1a** prefers to be a monomer in organic solvents and a dimer in water. The equilibrium distribution in favor of the dimer in water is reversed upon the addition of equivalent amounts of water-soluble hosts OA, CB,7 and CD to the aqueous solution. In the presence of the above hosts, the nitrosocumene **1a** exists as a monomer, despite its preference for dimer formation in pure water. Thus, a pronounced medium effect on the extent of nitrosocumene dimerization illustrates how a supramolecular concept can be used to alter the intermolecular dynamics in an aqueous solution. The ability of the cavitands to selectively bind the **1a** monomer in water could be useful in aqueous spin trap applications of nitrosobenzene, whose monomeric forms react with radicals but dimeric forms do not. Finally, the ability to resolve the two *N*-methyl NMR signals of **1b** upon freezing out C–NO and C–NMe₂ rotation within the OA capsule brings

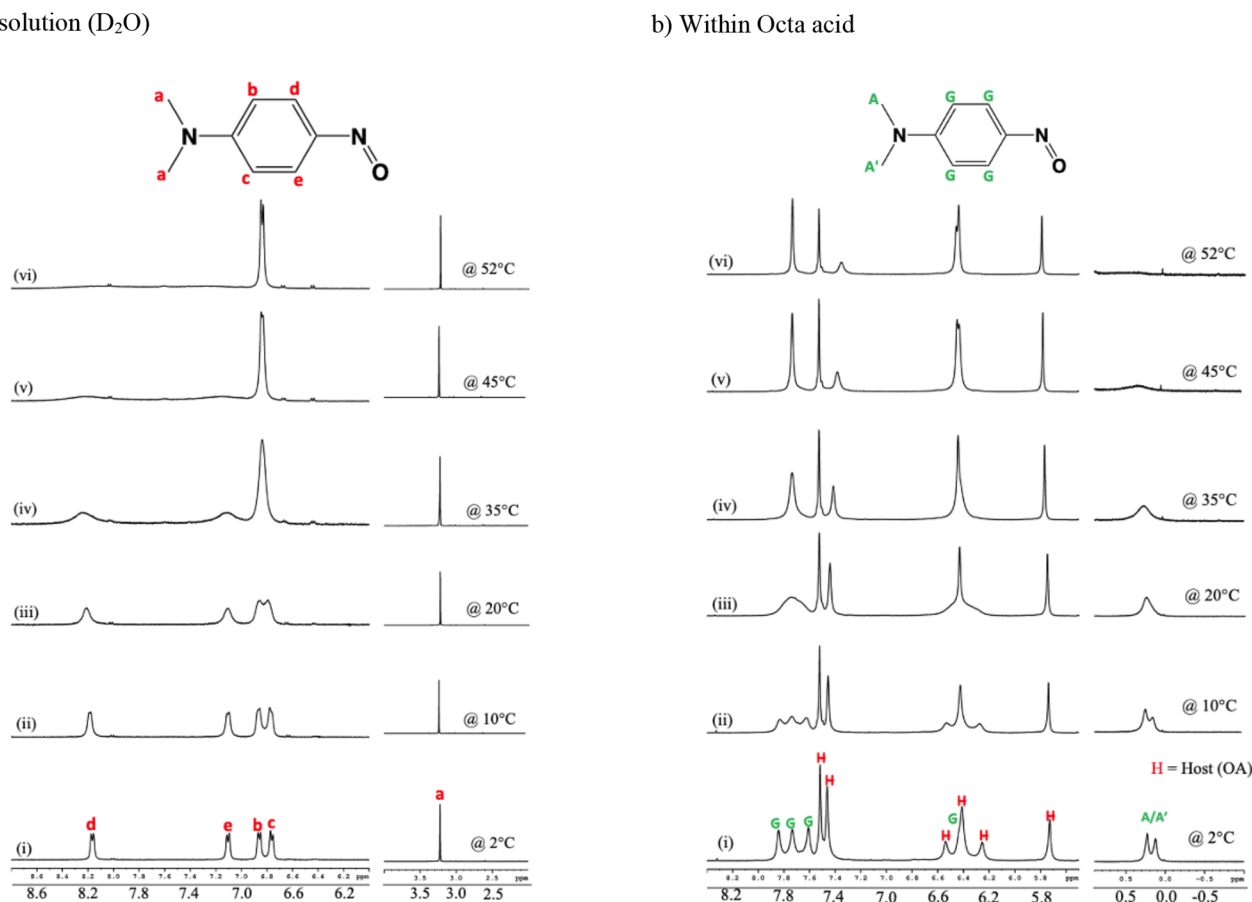


Figure 9. ^1H NMR spectra (500 MHz) of (a) **1b** in D_2O (1×10^{-3} M) and (b) **1b** (1×10^{-3} M) in octa acid (1×10^{-3} M) at (i) 2, (ii) 10, (iii) 20, (iv) 35, (v) 45, and (vi) 52 °C. Aromatic hydrogens were not individually assigned.

out the value of the phenomenon of supramolecular steric hindrance to modify the intramolecular dynamics of a guest molecule. The significant effects of supramolecular inclusion on the intermolecular aggregation state and intramolecular conformational dynamics are highlighted by the host–guest behavior of the nitrosobenzenes investigated in this study.

EXPERIMENTAL SECTION

General Information

All commercially available materials were used as supplied without further purification unless otherwise noted. NMR characterization, NMR titration studies, and diffusion experiments were performed on Bruker Avance 500 MHz spectrometer equipped with a cryoprobe and a Bruker 400 MHz spectrometer. Chemical shifts are reported in parts per million (ppm). Deuterated solvent was used as a lock, and the residual protiated solvent peak was used as a reference. Absorption spectra were recorded with a Shimadzu UV 3150 spectrophotometer.

Synthesis of Host and Guest Molecules

Octa acid (OA). Host octa acid was synthesized and characterized according to the reported procedure.⁴⁰

Cucurbit[7]uril (CB7). The optimized synthetic procedure was used to prepare CB7.^{41–43}

Cyclodextrin (CD). The hosts α -CD, β -CD, and γ -CD were obtained from Wacker Biochem Corp. and utilized as received.

***p*-Nitrosocumene (1a).** 4-Aminocumene (0.50 g, 3.7 mmol) was dissolved in DCM (10 mL) in a round-bottom flask equipped with a stir bar. Oxone (3.4 g, 5.6 mmol) was dissolved in water (20 mL) and added to the 4-aminocumene solution slowly via pipet. The reaction

mixture was vigorously stirred overnight and monitored by TLC (1:4 EtOAc/hexane) to verify the consumption of the starting material at 18 h. The DCM layer was then collected using a separatory funnel, and the aqueous layer extracted with DCM (3×15 mL). The combined organic layers were dried with anhydrous MgSO_4 , filtered, and concentrated in vacuo to give a dark green oil, which was purified through vaporization in a sublimation apparatus (0.06 mmHg, 80 °C) to yield a teal blue oil (0.083 g, 15%). ^1H NMR (360 MHz, CDCl_3): δ (ppm) 7.85 (d, $J = 8.3$ Hz, 2H), 7.45 (d, $J = 8.3$ Hz, 2H), 3.01 (sept, $J = 7.0$ Hz, 1H), 1.30 (d, $J = 7.0$ Hz, 6H).

***p*-Dimethyl Amino Nitrosobenzene (1b).** The guest **1b** was obtained from Alfa Aesar and recrystallized using 1:4 EtOAc/hexanes to give a bright green crystalline material (mp 88–90 °C, lit. 87–88 °C).⁴⁴

***p*-Nitrosocumene (1c).**¹² Compound **1c** was prepared by the synthetic method of Reddy as follows.⁴⁵ A solution of 4-isopropylaniline (0.81 g, 6.0 mmol, TCI America), potassium iodide (0.20 g, 1.2 mmol), and CH_3CN (18 mL) was added to a round-bottom flask and heated to 80 °C with stirring in an oil bath. To the solution was added 70% aqueous *tert*-butyl hydroperoxide (TBHP, 4.4 mL, 46 mmol) in small portions over 30 min with stirring via an addition funnel. A reflux condenser was then attached to the flask, and the reaction mixture was stirred at 80 °C overnight. The mixture was then cooled to room temperature and treated with 10 mL 10% KOH, washed with brine (1×10 mL), and extracted with ethyl acetate (2×15 mL). The combined organic layers were then dried with anhydrous MgSO_4 and concentrated in vacuo to give a dark red-brown oil, which was purified by column chromatography on silica gel using 1:30 EtOAc/hexanes to provide a mostly pure orange oil that was further purified by a second column on silica gel using 1:5 DCM/hexanes to give a light yellow oil (0.29 g, 32%). ^1H NMR (360 MHz, CDCl_3): δ (ppm) 8.17 (d, $J = 8.8$

Hz, 2H), 7.39 (d, $J = 8.8$ Hz, 2H), 3.14 (septet, $J = 6.8$ Hz, 1H), 1.30 (d, $J = 6.8$ Hz, 6H).

General Procedures for Sample Preparation

Monomer–dimer equilibrium in aqueous and nonaqueous media.

In Water. To the 0.6 mL of D₂O solution were added aliquots of the guest (**1a**) stock 60 mM solution (dissolved in DMSO-*d*₆) stepwise. After each addition, an NMR spectrum was collected to monitor the changes of the monomer and dimer proton resonances.

In Methanol, Dimethyl Sulfoxide, and Chloroform. To 0.6 mL of respective deuterated solvent solution were added aliquots of the guest (**1a**) stock 60 mM solution stepwise. After each addition, an NMR spectrum was collected to monitor the changes of the Monomer and Dimer proton resonances.

Compound 1a Dimer–Monomer Equilibrium Measurement in Water with a Sodium Acetate Internal Standard. An internal standard stock solution was made by dissolving anhydrous sodium acetate (0.0050 g) in 0.50 mL of D₂O. To an NMR tube was added 50 μ L of this solution via syringe, followed by an additional 0.55 mL of D₂O to give a total solution volume of 0.60 mL. A stock solution of **1a** was made by weighing out 0.0089 mL (0.0089 g, $d = 0.998$ g/mL) of *p*-nitrosocumene **1a** dissolved in 0.50 mL of DMSO-*d*₆ to give a 0.12 M solution. This solution was then added incrementally to the NMR tube in 5.0 μ L aliquots. ¹H NMR spectra were obtained on a 500 MHz NMR spectrometer; from 128 to 256 scans were acquired as needed to obtain a suitable signal-to-noise ratio. Concentrations of the **1a** monomer (M) and dimer (D) forms were determined by the relative integration to the known amount of internal standard according to $C_x = (I_x/I_{\text{cal}}) \times (N_{\text{cal}}/N_x) \times C_{\text{cal}}$ where I , N , and C are signal integral (area), the number of nuclei in the signal, and the molecule concentration, respectively. Experimental values of added **1a** (all forms), [M], [D], [NaOAc], total observed **1a** (all forms), and K_m are listed in Table 1. A resulting $\Delta G^\circ(298\text{ K}) = 20 \pm 1$ kJ/mol for monomerization was calculated from the average K_m value (0.00036 \pm 0.00016) at 300 K.

Inclusion of Guest Molecules Studied by ¹H NMR

Guest to Host Titration. To an NMR tube were added 0.6 mL of a D₂O stock solution of host OA (1 mM) and sodium borate buffer (10 mM). To this mixture were added aliquots of a DMSO-*d*₆ 60 mM respective guest stock solution stepwise. After each addition, an NMR spectrum was collected to monitor the changes of the host and guest proton resonances.

Host to Guest Titration (Reverse Titration). In D₂O was prepared a 2 mM solution of the respective guest solution. To this solution were added aliquots of a 20 mM host octa acid stock solution stepwise. After each addition, an NMR spectrum was collected to monitor the changes of the host and guest proton resonances.

With Cyclodextrins and Cucurbituril. In D₂O was prepared a 2 mM solution of the respective guest solution. To this solution were added aliquots of 5–40 mM respective host solution stock solution stepwise. After each addition, an NMR spectrum was collected to monitor the changes of the host and guest proton resonances.

***p*-Dimethylaminonitrosobenzene (1b) C–N Bond Rotation Evaluation in D₂O by VT-¹H-NMR (500 MHz).** Employing a nearly saturated solution of **1b** in D₂O, ¹H-NMR spectra were recorded at intervals between 2 and 77 °C. The sample temperature was evaluated using a methanol thermometer calibration curve for the spectrometer.⁴⁶ C–N rotational rate constants were calculated according to $k = (\pi/\sqrt{2})\Delta\nu$ at coalescence. Differences in signal chemical shifts ($\Delta\nu$, Hz) for the dynamically averaged Hs were obtained under “frozen out” conditions at 7 °C, and coalescence temperatures (Tcs) were estimated from spectral data in the 2–77 °C spectral data range. Values are reported in Table S2. The resulting ΔG^\ddagger values were calculated using the Eyring equation at Tcs.

Computational Methods

OA or CB7 small-molecule host–guest simulations were performed using the following multistep procedure. The 3D structure of OA was taken from our previous study,⁴⁷ and the crystal structure of CB7 was taken from the PDB structure (6SU0).⁴⁸ The guest molecules (*p*-

nitrosocumene and *p*-dimethylamino nitrosobenzene) were modeled using the Gauss View program. These structures were optimized without any geometrical constraints at the B3LYP^{49,50} or GD3BJ⁵¹ level utilizing the Gaussian 09 program package.⁵² In these calculations, the O and N atoms were treated with the 6-31+g(d) basis set, and C and H atoms were treated with the 6-31g(d) basis set.^{53,54} The RESP charges for OA, CB7, and guest molecules were calculated and used to create topology files using antechamber,^{55,56} an inbuilt tool in the Amber program. Specially, the SwissParam⁵⁷ tool was used to generate force field parameters for CB7. To build the initial structures of the host–guest complexes, a molecular docking procedure was performed using the AutoDock Vina ver. 1.5.6. program package.⁵⁸ The size of the grid was chosen to cover the hosts, and the spacing was kept to 1.00 Å. Each docking trial produced 20 poses with an exhaustiveness value equal to 20. The most promising poses provided by these docking procedures were subsequently used for MD simulations utilizing the GROMACS program^{59,60} and the AMBER03⁶¹ force field. For all simulations, the starting structures were placed in a cubic box with dimensions of 60 \times 60 \times 60 Å³. The remaining space of the box was filled with the TIP3P water molecules.⁶² Next, the system was neutralized by replacing some water molecules with sodium and chloride ions. These models were subsequently energy-minimized with a steepest descent method for 3000 steps to obtain starting structures for the subsequent MD simulations. All MD simulations were performed for 100 ns using a constant number of particles (N), pressure (P), and temperature (T), that is, the NPT ensemble. The LINCS⁶³ algorithm was used to constrain the bond lengths of the OA and CB7, whereas the SETTLE⁶⁴ program was used to constrain the bond lengths and angles of the water molecules. The long-range electrostatic interactions were calculated by the particle-mesh Ewald method.⁶⁵ A time step of 2 fs was used to compute the MD trajectories for each model. The most representative structures for host–guest complexes were derived from a cluster analysis. Molecular mechanics Poisson–Boltzmann surface area (MM-PBSA)⁶⁶ and lambda (λ) particle approach⁶⁷ methods were utilized to calculate the binding free energies of the host–guest complexation. Yasara,⁶⁸ Chimera,⁶⁹ and VMD⁷⁰ programs were used for the visualization and preparation of the structural diagrams presented in this study.

ASSOCIATED CONTENT

Supporting Information

The Supporting Information is available free of charge at <https://pubs.acs.org/doi/10.1021/acsorginorgau.1c00043>.

Experimental details, computational methods, computationally generated structures of host–guest complexes, and NMR and electronic absorption spectra of host–guest complexes (PDF)

AUTHOR INFORMATION

Corresponding Authors

Vaidhyanathan Ramamurthy – Department of Chemistry, University of Miami, Miami, Florida 33146, United States; orcid.org/0000-0002-3168-2185; Email: murthy@miami.edu

Silas C. Blackstock – Department of Chemistry and Biochemistry, The University of Alabama, Tuscaloosa, Alabama 35487-0336, United States; orcid.org/0000-0001-6733-9074; Email: blackstock@ua.edu

Authors

Ramkumar Varadharajan – Department of Chemistry, University of Miami, Miami, Florida 33146, United States
Sarah Ariel Kelley – Department of Chemistry and Biochemistry, The University of Alabama, Tuscaloosa, Alabama 35487-0336, United States

Vindi M. Jayasinghe-Arachchige – Department of Chemistry, University of Miami, Miami, Florida 33146, United States
Rajeev Prabhakar – Department of Chemistry, University of Miami, Miami, Florida 33146, United States; orcid.org/0000-0003-1137-1272

Complete contact information is available at:
<https://pubs.acs.org/10.1021/acsorginorgau.1c00043>

Notes

The authors declare no competing financial interest.

ACKNOWLEDGMENTS

V.R. and R.P. thank the National Science Foundation for financial support (CHE-1807729 and CHE-1664926, respectively).

REFERENCES

- (1) Lehn, J. M. *Supramolecular Chemistry*; Wiley VCH: Weinheim, Germany, 1995.
- (2) Brinker, U. H.; Mieusset, J.-L. *Molecular Encapsulation*; John Wiley & Sons: Chichester, England, 2010.
- (3) Voloshin, Y.; Belaya, I.; Kramer, R. *The Encapsulation Phenomenon*; Springer International Publishing: Switzerland, 2016.
- (4) Ramamurthy, V. Photochemistry within a Water-Soluble Organic Capsule. *Acc. Chem. Res.* **2015**, *48*, 2904–2917.
- (5) Szejtli, J.; Osa, T. *Cyclodextrins*, Vol. 3; Pergamon: Oxford, U.K., 1996.
- (6) Masson, E.; Ling, X.; Joseph, R.; Kyeremeh-Mensah, L.; Lu, X. Cucurbituril Chemistry: A Tale of Supramolecular Success. *RSC Adv.* **2012**, *2*, 1213–1247.
- (7) Vancik, H. *Aromatic C-Nitroso Compounds*; Springer, 2013; p 156.
- (8) Beaudoin, D.; Wuest, J. D. Dimerization of Aromatic C-Nitroso Compounds. *Chem. Rev. (Washington, DC, U. S.)* **2016**, *116*, 258–286.
- (9) Fehling, C.; Friedrichs, G. Dimerization of HNO in Aqueous Solution: An Interplay of Solvation Effects, Fast Acid-Base Equilibria, and Intramolecular Hydrogen Bonding? *J. Am. Chem. Soc.* **2011**, *133*, 17912–17922.
- (10) Rodenbough, P. P.; Karothu, D. P.; Gjorgjieva, T.; Commins, P.; Hara, H.; Naumov, P. Reversible Photolysis of Nitrosobenzene Cis-Dimer Monitored in Situ by Single Crystal Photocrystallography. *Cryst. Growth Des.* **2018**, *18*, 1293–1296.
- (11) Halasz, I.; Mestrovic, E.; Cicak, H.; Mihalic, Z.; Vancik, H. Solid-State Reaction Mechanisms in Monomer-Dimer Interconversions of p-Bromonitrosobenzene. *J. Org. Chem.* **2005**, *70*, 8461–8467.
- (12) Vančik, H.; Šimunić-Mežnarić, V.; Čaleta, I.; Meštrović, E.; Milovac, S.; Mlinarić-Majerski, K.; Veljković, J. Solid State Photochromism and Thermochromism in Nitroso Monomer-Dimer Equilibrium. *J. Phys. Chem. B* **2002**, *106*, 1576–1580.
- (13) Gowenlock, B. G.; Lüttke, W. Structure and Properties of C-Nitroso-Compounds. *Quarterly Reviews* **1958**, *12*, 321–340.
- (14) Fletcher, D. A.; Gowenlock, B. G.; Orrell, K. G. Structural Investigations of C-Nitrosobenzenes. *J. Chem. Soc., Perkin Trans. 2* **1997**, 2201–2206.
- (15) Fletcher, D. A.; Gowenlock, B. G.; Orrell, K. G. Structural Investigations of C-Nitrosobenzenes. *J. Chem. Soc., Perkin Trans. 2* **1998**, 797–804.
- (16) Orrell, K. G.; Sik, V.; Stephenson, D. Study of the Monomer-Dimer Equilibrium of Nitrosobenzene Using Multinuclear One- and Two-Dimensional NMR Techniques. *Magn. Reson. Chem.* **1987**, *25*, 1007–11.
- (17) Tanford, C. *The Hydrophobic Effect: Formation of Micelles and Biological Membranes*, 2nd ed.; John Wiley & Sons: New York, NY, 1980.
- (18) Otto, S.; Engberts, J. B. F. N. Diels-Alder Reactions in Water. *Pure Appl. Chem.* **2000**, *72*, 1365–1372.
- (19) Glaser, R.; Murmann, R. K.; Barnes, C. L. Why Do Nitroso Compounds Dimerize While Their Oxime Tautomers Do Not? A Structural Study of the Trans-Dimer of 2-Chloro-2-Methyl-3-Nitrosobutane and Higher Level Ab Initio Study of Thermodynamic Stabilities and Electronic Structures of Isomers of Diazene Dioxides. *J. Org. Chem.* **1996**, *61*, 1047–1058.
- (20) Grieco, P. A.; Garner, P.; He, Z. Micellar Catalysis in the Aqueous Intermolecular Diels-Alder Reaction: Rate Acceleration and Enhanced Selectivity. *Tetrahedron Lett.* **1983**, *24*, 1897–1900.
- (21) Grieco, P. A.; Garner, P.; He, Z.-M. Micellar Catalysis in the Aqueous Intermolecular Diels-Alder Reaction: Rate Acceleration and Enhanced Selectivity. *Tetrahedron Lett.* **1983**, *24*, 1897–1900.
- (22) Grieco, P. A.; Nunes, J. J.; Gaul, M. D. Dramatic Rate Accelerations of Diels-Alder Reactions in 5 M Lithium Perchlorate-Diethyl Ether: The Cantharidin Problem Reexamined. *J. Am. Chem. Soc.* **1990**, *112*, 4595–4596.
- (23) Breslow, R. Hydrophobic Effects on Simple Organic Reactions in Water. *Acc. Chem. Res.* **1991**, *24*, 159–164.
- (24) Breslow, R. Determining the Geometries of Transition States by Use of Antihydrophobic Additives in Water. *Acc. Chem. Res.* **2004**, *37*, 471–478.
- (25) Breslow, R. The Hydrophobic Effect in Reaction Mechanism Studies and in Catalysis by Artificial Enzymes. *J. Phys. Org. Chem.* **2006**, *19*, 813–822.
- (26) Breslow, R. *A Fifty-Year Perspective on Chemistry in Water*; Blackwell: Hoboken, NJ, 2007.
- (27) Otto, S.; Engberts, J. B. F. N. Hydrophobic Interactions and Chemical Reactivity. *Org. Biomol. Chem.* **2003**, *1*, 2809–2820.
- (28) Jung, Y.; Marcus, R. A. On the Theory of Organic Catalysis “on Water”. *J. Am. Chem. Soc.* **2007**, *129*, 5492–5502.
- (29) Narayan, S.; Fokin, V. V.; Sharpless, K. B. *Chemistry ‘On Water’ - Organic Synthesis in Aqueous Suspension*; Blackwell: Hoboken, NJ, 2007.
- (30) Narayan, S.; Muldoon, J.; Finn, M. G.; Fokin, V. V.; Kolb, H. C.; Sharpless, K. B. On Water: Unique Reactivity of Organic Compounds in Aqueous Suspension. *Angew. Chem., Int. Ed.* **2005**, *44*, 3275–3279.
- (31) Jayaraj, N.; Zhao, Y.; Parthasarathy, A.; Porel, M.; Liu, R. S. H.; Ramamurthy, V. Nature of Supramolecular Complexes Controlled by the Structure of the Guest Molecules: Formation of Octa Acid Based Capsuleplex and Cavitandplex. *Langmuir* **2009**, *25*, 10575–10586.
- (32) Choudhury, R.; Barman, A.; Prabhakar, R.; Ramamurthy, V. Hydrocarbons Depending on the Chain Length and Head Group Adopt Different Conformations within a Water-Soluble Nanocapsule: ¹H NMR and Molecular Dynamics Studies. *J. Phys. Chem. B* **2013**, *117*, 398–407.
- (33) Gibb, C. L. D.; Gibb, B. C. Binding of Cyclic Carboxylates to Octa-Acid Deep-Cavity Cavitand. *J. Comput.-Aided Mol. Des.* **2014**, *28*, 319–325.
- (34) Hoffmann, R.; Gleiter, R.; Mallory, F. B. Non-Least-Motion Potential Surfaces. *J. Am. Chem. Soc.* **1970**, *92*, 1460–1466.
- (35) Lüttke, W.; Skancke, P. N.; Traetteberg, M. On the dimerization process of nitroso compounds. *Ther. Chim. Acta* **1994**, *87*, 321–333.
- (36) Ruud, K.; Helgaker, T.; Uggerud, E. Mechanisms, energetics and dynamics of a key reaction sequence during the decomposition of nitromethane: HNO + HNO → N₂O + H₂O. *J. Mol. Struct.: THEOCHEM* **1997**, *393*, 59–71.
- (37) Varga, K.; Biljan, I.; Tomišić, V.; Mihalić, Z.; Vančik, H. *J. Phys. Chem. A* **2018**, *122*, 2542–2549.
- (38) Porel, M.; Jayaraj, N.; Kaanumalle, L. S.; Maddipatla, M. V. S. N.; Parthasarathy, A.; Ramamurthy, V. Cavitand Octa Acid Forms a Nonpolar Capsuleplex Dependent on the Molecular Size and Hydrophobicity of the Guest. *Langmuir* **2009**, *25*, 3473–3481.
- (39) Furness, A. R.; Buckley, P. D.; Jolley, K. W. Effect of the Solvent on the Barrier to Internal Rotation in p-Substituted Nitrosoanilines. *Aust. J. Chem.* **1975**, *28*, 2303–6.

- (40) Gibb, C. L.; Gibb, B. C. Well-defined, organic nanoenvironments in water: The hydrophobic effect drives a capsular assembly. *J. Am. Chem. Soc.* **2004**, *126*, 11408–11409.
- (41) Behrend, R.; Meyer, E.; Rusche, F. I. Ueber condensationsproducte aus glycoluril und formaldehyd. *Justus Liebigs Ann. Chem.* **1905**, *339*, 1–37.
- (42) Freeman, W.; Mock, W.; Shih, N. Cucurbituril. *J. Am. Chem. Soc.* **1981**, *103*, 7367–7368.
- (43) Kim, J.; Jung, I.-S.; Kim, S.-Y.; Lee, E.; Kang, J.-K.; Sakamoto, S.; Yamaguchi, K.; Kim, K. New cucurbituril homologues: syntheses, isolation, characterization, and X-ray crystal structures of cucurbit [n]uril (n = 5, 7, and 8). *J. Am. Chem. Soc.* **2000**, *122*, 540–541.
- (44) Hashimoto, T. [Synthesis of organosilicon compounds. *Yakugaku Zasshi* **1967**, *87*, 291–295.
- (45) Reddy, K. R.; Maheswari, C. U.; Venkateshwar, M.; Kantam, M. L. Selective oxidation of aromatic amines to nitro derivatives using potassium iodide-tert-butyl hydroperoxide catalytic system. *Adv. Synth. Catal.* **2009**, *351*, 93–96.
- (46) Van Geet, A. L. Calibration of methanol nuclear magnetic resonance thermometer at low temperature. *Anal. Chem.* **1970**, *42*, 679–680.
- (47) Kulasekharan, R.; Choudhury, R.; Prabhakar, R.; Ramamurthy, V. Restricted rotation due to the lack of free space within a capsule translates into product selectivity: photochemistry of cyclohexyl phenyl ketones within a water-soluble organic capsule. *Chem. Commun.* **2011**, *47*, 2841–2843.
- (48) Guagnini, F.; Engilberge, S.; Ramberg, K. O.; Pérez, J.; Crowley, P. B. *Chem. Commun.* **2020**, *56*, 360–363.
- (49) Becke, A. D. Density-functional exchange-energy approximation with correct asymptotic behavior. *Phys. Rev. A: At., Mol., Opt. Phys.* **1988**, *38*, 3098.
- (50) Becke, A. Density-functional thermochemistry. III. The role of exact exchange. *J. Chem. Phys.* **1993**, *98*, 5648–5652.
- (51) Grimme, S.; Ehrlich, S.; Goerigk, L. Effect of the damping function in dispersion corrected density functional theory. *J. Comput. Chem.* **2011**, *32*, 1456–1465.
- (52) Frisch, M.; Trucks, G.; Schlegel, H.; Scuseria, G.; Robb, M.; Cheeseman, J.; Scalmani, G.; Barone, V.; Mennucci, B.; Petersson, G.; et al. *Gaussian 09*, rev. D.01; Gaussian, Inc.: Wallingford, CT, 2009.
- (53) Francl, M. M.; Pietro, W. J.; Hehre, W. J.; Binkley, J. S.; Gordon, M. S.; DeFrees, D. J.; Pople, J. A. Self-consistent molecular orbital methods. *J. Chem. Phys.* **1982**, *77*, 3654–3665.
- (54) Rassolov, V. A.; Ratner, M. A.; Pople, J. A.; Redfern, P. C.; Curtiss, L. A. 6-31G* basis set for third-row atoms. *J. Comput. Chem.* **2001**, *22*, 976–984.
- (55) Wang, J.; Wang, W.; Kollman, P. A.; Case, D. A. Automatic atom type and bond type perception in molecular mechanical calculations. *J. Mol. Graphics Modell.* **2006**, *25*, 247–260.
- (56) Wang, J.; Wolf, R. M.; Caldwell, J. W.; Kollman, P. A.; Case, D. A. Development and testing of a general amber force field. *J. Comput. Chem.* **2004**, *25*, 1157–1174.
- (57) Zoete, V.; Cuendet, M. A.; Grosdidier, A.; Michielin, O. J. J. O. C. C. *J. Comput. Chem.* **2011**, *32*, 2359–2368.
- (58) Trott, O.; Olson, A. J. AutoDock Vina: Improving the speed and accuracy of docking with a new scoring function, efficient optimization, and multithreading. *J. Comput. Chem.* **2010**, *31* (2), 455–461.
- (59) Pronk, S.; Páll, S.; Schulz, R.; Larsson, P.; Bjelkmar, P.; Apostolov, R.; Shirts, M. R.; Smith, J. C.; Kasson, P. M.; van der Spoel, D.; et al. GROMACS 4.5: A high-throughput and highly parallel open source molecular simulation toolkit. *Bioinformatics* **2013**, *29*, 845–854.
- (60) Hess, B.; Kutzner, C.; Van Der Spoel, D.; Lindahl, E. GROMACS 4: algorithms for highly efficient, load-balanced, and scalable molecular simulation. *J. Chem. Theory Comput.* **2008**, *4*, 435–447.
- (61) Case, D. A.; Cheatham III, T. E.; Darden, T.; Gohlke, H.; Luo, R.; Merz Jr, K. M.; Onufriev, A.; Simmerling, C.; Wang, B.; Woods, R. J. The Amber biomolecular simulation programs. *J. Comput. Chem.* **2005**, *26*, 1668–1688.
- (62) Price, D. J.; Brooks III, C. L. A modified TIP3P water potential for simulation with Ewald summation. *J. Chem. Phys.* **2004**, *121*, 10096–10103.
- (63) Hess, B.; Bekker, H.; Berendsen, H. J.; Fraaije, J. G. LINCS: a linear constraint solver for molecular simulations. *J. Comput. Chem.* **1997**, *18*, 1463–1472.
- (64) Miyamoto, S.; Kollman, P. A. Settle: An analytical version of the SHAKE and RATTLE algorithm for rigid water models. *J. Comput. Chem.* **1992**, *13*, 952–962.
- (65) Darden, T.; York, D.; Pedersen, L. Particle mesh Ewald: An N-log(N) method for Ewald sums in large systems. *J. Chem. Phys.* **1993**, *98*, 10089–10092.
- (66) Kumari, R.; Kumar, R.; Lynn, A. *g_mmpbsa* - A GROMACS tool for high-throughput MM-PBSA calculations. *J. Chem. Inf. Model.* **2014**, *54*, 1951–1962.
- (67) Knight, J. L.; Brooks III, C. L. λ -Dynamics free energy simulation methods. *J. Comput. Chem.* **2009**, *30*, 1692–1700.
- (68) Krieger, E.; Vriend, G. Models@ Home: distributed computing in bioinformatics using a screensaver based approach. *Bioinformatics* **2002**, *18*, 315–318.
- (69) Pettersen, E. F.; Goddard, T. D.; Huang, C. C.; Couch, G. S.; Greenblatt, D. M.; Meng, E. C.; Ferrin, T. E. UCSF Chimera—a visualization system for exploratory research and analysis. *J. Comput. Chem.* **2004**, *25*, 1605–1612.
- (70) Humphrey, W.; Dalke, A.; Schulten, K. VMD: visual molecular dynamics. *J. Mol. Graphics* **1996**, *14*, 33–38.